Polymer 52 (2011) 2899–2909

Contents lists available at ScienceDirect

Polymer

journal homepage: www.elsevier.com/locate/polymer

An experimental and theoretical investigation of the compressive properties of multi-walled carbon nanotube/poly(methyl methacrylate) nanocomposite foams

Limeng Chen [a,b], Linda S. Schadler [a,b], Rahmi Ozisik [a,b,*]

[a] Department of Materials Science and Engineering, Rensselaer Polytechnic Institute, 110 8th Street, Troy, NY 12180, United States
[b] Rensselaer Nanotechnology Center, Rensselaer Polytechnic Institute, 110 8th Street, Troy, NY 12180, United States

ARTICLE INFO

Article history:
Received 29 March 2011
Received in revised form
21 April 2011
Accepted 26 April 2011
Available online 6 May 2011

Keywords:
Carbon nanotubes
Polymer nanocomposite foams
Compressive properties

ABSTRACT

Polymer nanocomposite foams are promising low density substitutes for nanocomposites. Carbon nanotube/polymer nanocomposite foams possess high strength, low density, and can be made conductive. Good control of foam properties is of great importance in the application of such materials. In the current study, multi-walled carbon nanotubes (MWNTs) with controlled aspect ratio were used to alter the foam morphology in MWNT/poly(methyl methacrylate) (PMMA) nanocomposite foams produced by a supercritical carbon dioxide (CO_2) foaming process. It was found that with the addition of one weight percent of MWNTs, the Young's modulus of polymer foams increased by as much as 82%, and the collapse strength increased by as much as 104%. The influence of MWNT aspect ratio on the compressive properties of nanocomposite foams was investigated. The addition of MWNTs influenced the foam properties in two ways: improving the compressive properties of the solid matrix, and reducing the bubble size of the nanocomposite foams. A modified constitutive model for predicting the compressive properties of high density closed-cell polymer foams was developed. The influence of the bubble size on the mechanical properties of polymer foams was discussed based on the new model.

1. Introduction

Polymer nanocomposite foams, products from the foaming of polymer nanocomposites, have received increasing attention in both the scientific and industrial communities. The combination of functional nanofillers and foaming technology has a high potential to generate a new class of materials that are light, strong, and multifunctional. A small amount of well-dispersed nanofillers in a polymer matrix has been shown to serve as sites to facilitate bubble nucleation [1]. In addition, nanoscale particles can increase the modulus and strength of polymers [1,2]. Siripurapu et al. [3] studied the morphology of silica/poly(methyl methacrylate) nanocomposites foamed by supercritical carbon dioxide (CO_2). With increasing loading of well-dispersed nanosilica particles, the bubble density increased, and as a result, the bubble size decreased. Zhai et al. [4] showed that the addition of nanosilica into polymers could lead to uniform bubble size in the foamed structure. With the presence of fillers, more bubbles start to nucleate concurrently, resulting in less gas for bubble growth, leading to a reduction of bubble size [5]. In addition, fillers increase the shear viscosity of polymer melts, which hinders bubble growth [6].

Low density is one of the most attractive properties of polymer foams as a light weight substitute for structural or functional materials. However, the mechanical properties of polymer foams are almost always compromised after density reduction [7,8]. A combination of light weight and high strength has always been the major research objective in the research area of polymer foams. The mechanical properties of polymer foams not only depend on the intrinsic properties of the polymer, but also on the microstructure of the foam, such as bubble density, bubble size and bubble size distribution [8,9]. Alvarez et al. [9], by using finite element modeling, predicted that the compressive elastic modulus showed a linear relationship with relative density of polymer foams when the relative bubble density is higher than 0.5. Their results agreed well with the experimental results of Saint-Michel et al. [10]. Kabir et al. [11] studied the tensile and mode-I fracture behavior of cross-linked polyvinyl chloride and rigid polyurathene foam, and found that the foam density and solid polymer intrinsic properties had a significant influence on tensile strength, modulus and fracture toughness of polymer foams.

Nanofillers are commonly used to reinforce polymer foams. Saha et al. [12] found that with the addition of 0.5 weight percent carbon nanofibers, the mode-I fracture toughness of rigid polyurethane

* Corresponding author. Department of Materials Science and Engineering, Rensselaer Polytechnic Institute, 110 8th Street, Troy, NY 12180, United States. Tel.: +1 518 276 6786.
E-mail address: ozisik@rpi.edu (R. Ozisik).

0032-3861/$ – see front matter © 2011 Elsevier Ltd. All rights reserved.
doi:10.1016/j.polymer.2011.04.050

foams increased by 28%. They proposed that the smaller bubble size, due to the addition of carbon nanofibers, reduced the effective bending stress on neighboring bubbles around the crack. In addition, the presence of dispersed nanoparticles at the edge of a bubble could act as crack arrest centers by creating multiple crack branching that could delay crack propagation. Mahfuz et al. [13] found that the addition of three weight percent of TiO_2 nanoparticles significantly increased (50–70%) the flexural strength and stiffness of polyurethane nanocomposite foams. The tensile properties of extruded polystyrene/carbon nanofiber composites were investigated by Shen et al. [14]. They found that the tensile modulus of polystyrene foams increased with increasing concentration of carbon nanofibers (CNF). When the fiber concentration reached 5% by weight, the tensile modulus of the CNF/polystyrene nanocomposite foams with a density of 0.69 g/cm^3 was 1.07 GPa, which is comparable to that of solid polystyrene (1.26 GPa).

Conductive polymer nanocomposite foams filled with carbon nanotubes have been receiving increasing attention. Such foams possess most of the properties of solid carbon nanotube/polymer nanocomposites such as high electrical conductivity and enhanced mechanical properties but at reduced weight [15,16]. Their superior properties as effective electromagnetic interference shielding materials have been well studied [17,18].

The influence of carbon nanotube properties such as aspect ratio and surface chemistry on the properties of solid polymer nanocomposites has been previously reported [15,18]. However, carbon nanotube/polymer nanocomposite foams are more complex than their solid composites. The interactions between fillers, bubbles and matrix polymer and their influence on the properties of nanocomposite foams are still not fully understood. In addition, the properties of one component may affect the properties of the other two [19]. In our recent paper [19], we showed that the aspect ratio of multi-walled carbon nanotubes (MWNT) had a significant influence on the foam morphology of MWNT/polymer nanocomposite foams. At constant MWNT concentration, nanocomposite foams filled with short MWNTs had greater bubble density and smaller bubble size than nanocomposite foams filled with long MWNTs. The aspect ratio of MWNTs has been shown to influence the mechanical properties of solid nanocomposites as well [20]. To achieve good control over the mechanical properties of MWNT/polymer nanocomposite foams, it is important to understand the influence of MWNT aspect ratio on the mechanical properties of the polymer nanocomposite foams.

In the current study, poly(methyl methacrylate), PMMA, and MWNT/PMMA nanocomposites containing MWNT with controlled aspect ratios were foamed with supercritical CO_2 at various conditions to generate foams with different density. Supercritical CO_2 was chosen as the physical foaming agent due to its relatively low critical temperature (31 °C), low critical pressure (7.38 MPa) and non-toxic nature. Compression tests were done on all nanocomposite foams and neat PMMA foams. The Young's modulus and collapse strength of different samples were compared. In this paper, the influence of MWNTs and MWNT aspect ratio on the compressive properties of PMMA foams is discussed. A modified constitutive model for predicting the change of compressive properties of foams with the change of foam density is proposed.

2. Experimental

2.1. Materials

MWNTs were synthesized at Rensselaer using a chemical vapor deposition method on silicon wafers [21]. MWNTs with varying lengths but similar diameters (~30 nm) were obtained by controlling the growth time. The growth rate was found to be approximately 1 μm/min. Thermogravimetric analysis (TGA) of MWNTs indicated that there was less than 4.3% (by weight) catalyst in the samples.

Poly(methyl methacrylate), PMMA, was chosen as the composite matrix polymer because of its outstanding chemico-physical properties [22] and relatively high affinity for CO_2. Commercial grade PMMA (Plexiglas V920-100) was kindly donated by Altuglas International. Glycidyl phenyl ether (GPE) and trihexylamine were purchased from Acros Organics. Tetrahydrofuran (THF) and concentrated nitric acid (HNO_3, 70%) were purchased from Sigma–Aldrich, and ethyl alcohol was purchased from Fisher Scientific.

2.2. MWNT surface oxidization

In order to obtain a good dispersion of MWNTs in PMMA, MWNTs were first treated with concentrated nitric acid to remove any amorphous carbon on the tube walls and to introduce carboxyl groups to the surface [23]. In a typical experiment, 100 mg of MWNT was immersed in 200 mL of concentrated nitric acid inside a 250 mL round bottom flask. A water-cooled condenser was attached to the flask and the mixture was heated to maintain boiling in a refluxing system for 2 h. The mixture was allowed to cool to room temperature and then the oxidized MWNTs were washed by dispersing in water and filtering with poly(tetrafluoroethylene) (PTFE) membranes with 0.4 μm pore size multiple times. Finally, the oxidized MWNTs were dispersed in water and freeze-dried. MWNTs of two different aspect ratios were oxidized, one was grown for 20 min with an average aspect ratio of 677 (*MWNT20*), and the other was grown for 100 min with an average aspect ratio of 3334 (*MWNT100*).

2.3. Preparation of MWNT/PMMA nanocomposites

Solution-mixing method was chosen to prepare the MWNT/PMMA nanocomposites because it leads to good dispersion of MWNTs and does not cause significant damage to the MWNTs. All nanocomposites contained 1% (by weight) MWNT. In a typical experiment, 2 g of PMMA was dissolved in 100 mL THF by bath sonication for 2 h; 20 mg of oxidized MWNT was dispersed in 50 mL anhydrous THF by water bath sonication for 6 min, followed by ultrasonication with a wand sonicator for 30 s. The MWNT/THF dispersion and the PMMA/THF solution were mixed by ultrasonicating with a wand sonicator for 1 min. The mixture was poured into a large quantity of ethanol stirred by a magnetic bar to facilitate precipitation. The volume ratio of THF to ethanol was 1:5.

Control samples made of neat PMMA were also prepared. In a typical experiment, as-received PMMA was dissolved in THF by bath sonication for 2 h and 6 min (the same duration as the composite samples). Then the solution was ultrasonicated with a wand sonicator for 1 min. The solution was poured into a large quantity of ethanol stirred by a magnetic bar so that the PMMA precipitated out.

The precipitates were filtered with a PTFE membrane and dried under vacuum at 70 °C for 24 h. The dried nanocomposites were compounded into rectangular shapes (5.08 cm × 0.635 cm × 0.5 cm) with a hot press at 225 °C under 19.6 kN of load and were cooled down to room temperature. Two types of composites were prepared by this method: one with oxidized MWNT grown for 100 min (*C100*) and the second with oxidized MWNT grown for 20 min (*C20*).

Transmission electron microscopy (TEM) was used to investigate the dispersion of MWNTs in PMMA. The samples were cut with a microtome to a thickness of 70 nm at room temperature with a diamond knife and mounted on a 200-mesh copper grid. Images were obtained with a Phillips CM12 using an accelerating voltage of 120 kV.

2.4. Foaming nanocomposites with supercritical carbon dioxide

A batch foaming process was used to make MWNT/PMMA nanocomposite foams. A customized supercritical CO_2 foaming setup was assembled and used for foaming the mechanical testing samples. A tubular Micro Reactor from High Pressure Equipment Company was connected to a syringe pump. An insulated heating band was wrapped around the outer surface of the reactor and the temperature was controlled via a thermal couple inserted into the reactor for precise control.

To investigate the influence of MWNT aspect ratio on the compressive properties of the nanocomposite foams, nanocomposites *C100* and *C20* and neat PMMA control samples were soaked in supercritical CO_2 under varying soaking temperatures and constant pressure (17.9 MPa) for 24 h. After fast pressure release ($\sim$10 MPa/s), the samples were taken out of the autoclave and immersed in ice water. Four different soaking temperatures were used: 65, 85, 100 and 125 °C. The foamed nanocomposites *C100* and *C20* were named as *F-C100* and *F-C20*, respectively.

2.5. Bubble density analysis

Field emission scanning electron microscope (FESEM) was used for bubble density analysis. Samples were freeze-fractured in liquid nitrogen and the fracture surface was sputter-coated with gold. Typically, a micrograph showing more than 100 bubbles was chosen. Bubble density and bubble size analysis was conducted using ImageJ (National Institute of Health). The number of bubbles (n) was counted from a collection of images. The number of bubbles per unit volume (N) was calculated using the following equation:

$$N = \left(\frac{nM^2}{A}\right)^{3/2} \quad (1)$$

where A is the area of the FESEM image and M is the magnification factor.

2.6. Compression testing of nanocomposites and nanocomposite foams

Compression tests were carried out according the ASTM standard D1621-04a. All solid nanocomposites, nanocomposite foams, and neat PMMA control samples were cut by Buehler Isomet diamond saw into cubic specimens with dimensions of 5 mm × 5 mm × 5 mm for compression testing. The specimens were kept inside a desiccator for 24 h and were thoroughly dried before the apparent density was measured. The apparent density was calculated by dividing the mass of the specimen by the volume of the specimen. The density of five specimens for each type of sample was averaged to get the average density of the samples.

The compression tests of solid specimens were done on an Instron 4202 machine with a 50 kN load cell at room temperature. The compression tests of foams were done on an Instron 5843 tabletop tester with a 1 kN load cell at room temperature. The strain rate was held constant at 0.05 min^{-1}. Five specimens were tested for each sample.

It should be noted that for the compression tests of solid samples, the specimen geometry is cubic with edge length of 5 mm, while the ASTM standard test method for compressive properties of rigid polymers (D695-02a) requires that the test specimen be in the form of a right cylinder or prism whose length is twice its principal diameter or width. The cubic geometry was chosen because the solid samples were deemed as foams with a relative density of one, i.e. foams with the same density as the density of bulk polymer. The sample geometry complied with the ASTM standard test method for the compressive properties of rigid cellular plastics (D1621-04a). Because of the cubic geometry of the specimens, the specimens did not fracture during the test. Instead, the specimens were compressed into thin right square prisms. The tests were manually stopped when 50% strain was reached.

3. Results and discussion

3.1. Dispersion of MWNTs in PMMA

Typical TEM images of the nanocomposites *C100* and *C20* are shown in Fig. 1. The images indicate good dispersion and no agglomeration of both types of MWNT in PMMA.

3.2. The foam morphology of polymer nanocomposite foams

The foam morphology of *F-C100*, *F-C20* and neat PMMA foamed with supercritical CO_2 at 17.9 MPa at four different temperatures of 65 °C, 80 °C, 100 °C and 125 °C were characterized by FESEM. Typical FESEM images are presented in Fig. 2. Bubble density and bubble size analysis was done with ImageJ and the results are shown in Fig. 3 and Table 1. The nanocomposite samples (*F-C100* and *F-C20*) had greater bubble density and smaller average bubble size than those of neat PMMA foams. The average bubble size decreased with increasing

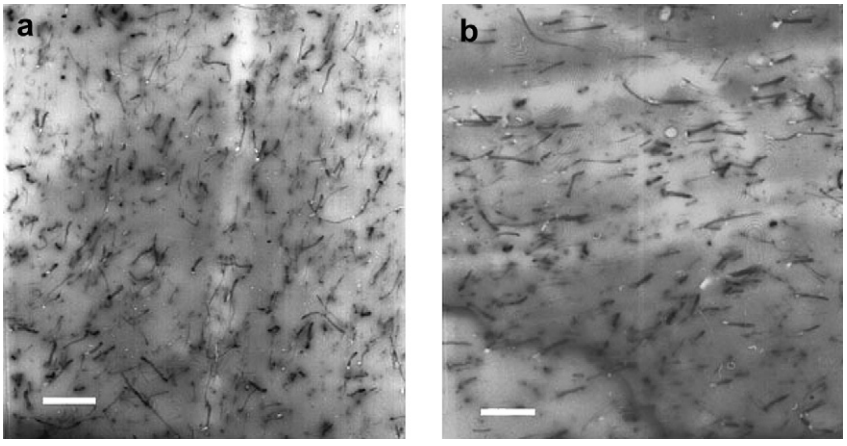

Fig. 1. TEM images of MWNTs dispersed in nanocomposites: (a) *C20* (b) *C100*, scale bar = 1 μm.

bubble density as expected [19]. In general, the bubble density decreased and the average bubble size increased with increasing saturation temperature. *F-C20* foams had greater bubble density and smaller average bubble size than *F-C100* foams irrespective of the saturation temperature at 17.9 MPa saturation pressure. However, the difference between *F-C100* and *F-C20* foam structures became smaller with increasing saturation temperature.

3.3. Compressive properties of PMMA and MWNT/PMMA nanocomposites

Typical compressive stress–strain curves for neat PMMA and *C100* and *C20* nanocomposites are shown in Fig. 4 along with the Young's modulus and compressive strength. It can be seen that the addition of MWNTs increased both the elastic modulus and compressive strength of the PMMA. The addition of 1% of *MWNT100* increased the Young's modulus by ~40% and the compressive strength by ~14%. On the other hand, the addition of 1% of *MWNT20* increased the Young's modulus by ~8% and the compressive strength by ~7%.

The mechanical enhancement of polymers by MWNTs has been extensively studied [15,24]. The increase in the Young's modulus and compressive strength of nanocomposites was primarily attributed to the presence of a large volume fraction of interphase

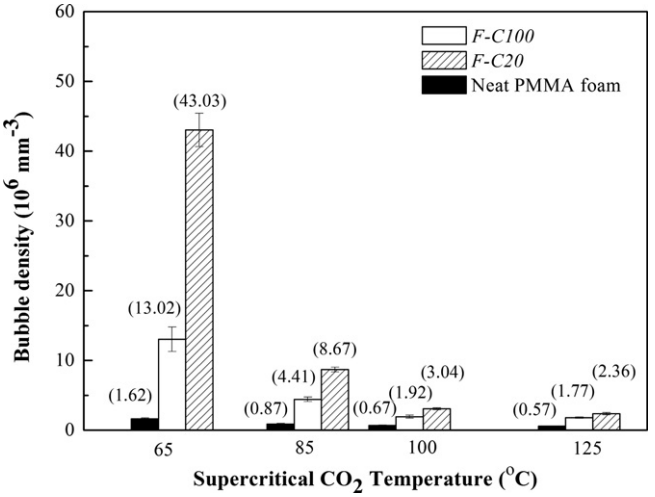

Fig. 3. A comparison of the bubble density of neat PMMA, *C100*, and *C20* nanocomposites foamed with supercritical CO_2 at 17.9 MPa at four different temperatures. The error bars represent the standard deviations of the bubble density data for five samples under each condition.

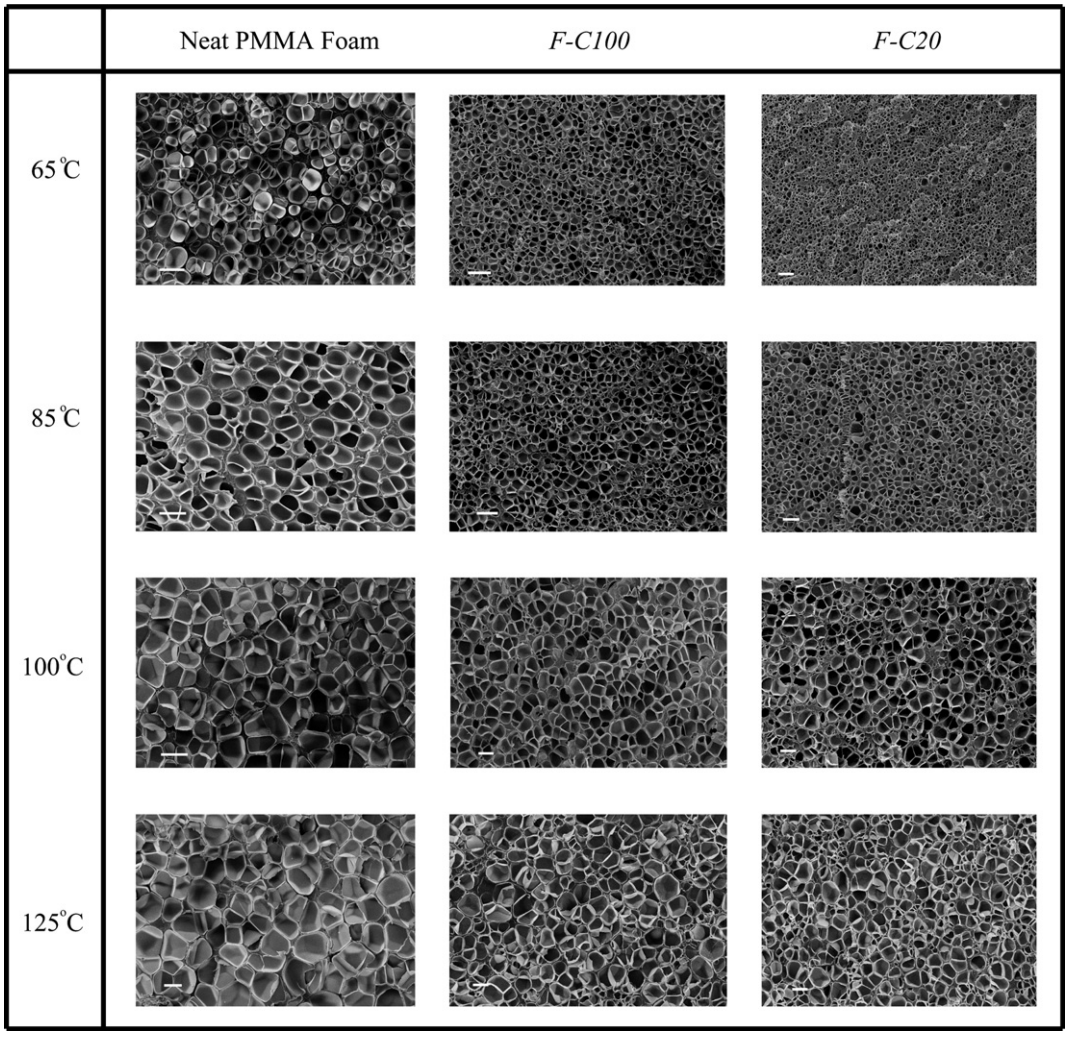

Fig. 2. Typical FESEM images of neat PMMA, *C100* and *C20* foams foamed with supercritical CO_2 at 17.9 MPa and different temperatures. Scale bar = 10 μm.

Table 1
Average cell radii of nanocomposites *F-C100*, *F-C20* and *F*-PMMA foamed under various conditions.

Temperature (°C)	Average bubble radius (μm)		
	F-PMMA	*F-C100*	*F-C20*
65	4.94	2.42	1.34
85	6.76	3.94	3.15
100	8.18	5.44	4.57
125	8.93	5.82	5.07

with altered polymer mobility at the polymer–nanofiller interface [24]. However, in the current study, the differences in the Young's modulus and compressive strength of *C100* and *C20* can only be due to the aspect ratio of MWNTs used. Greater aspect ratio leads to better load transfer between the polymer matrix and the MWNTs [25].

3.4. Compressive properties of the foams

Foaming of neat PMMA and MWNT/PMMA nanocomposites leads to drastic changes in the density of the material and affects the mechanical properties. The relative density, the apparent foam density divided by the unfoamed density (1.18 g/cm^3), of the foamed samples is presented in Fig. 5. The major factor affecting the relative density of the foams is the saturation temperature; as the supercritical CO_2 saturation temperature increased, the relative density decreased irrespective of sample type (neat PMMA vs. MWNT filled PMMA). And although the effect is small, the relative density is greater for MWNT filled samples than neat PMMA. In addition, the relative density of the *F-C100* foam is greater than that of *F-C20* foam.

Typical compressive stress–strain curves of *F-C100* and *F-C20* nanocomposite foams and neat PMMA foam at four different saturation temperatures are presented in Fig. 6. The elastic modulus and the collapse strength of the foams as a function of relative density are presented in Fig. 7. It can be seen that the nanocomposite foams have greater modulus and collapse strength than the neat PMMA foam at all saturation temperatures. In general the use of MWNT and in particular the use of longer MWNTs led to increased properties. For example, the addition of only 1% of *MWNT100* led to 82% increase in the Young's modulus and 104% increase in the collapse strength (at a relative density of 0.5). Both the modulus and the collapse strength decreased with decreasing relative density as expected.

In general, the mechanical properties of polymer foams not only depend on the mechanical properties of the matrix material, but also depend on the density (or the relative density) of the foam and the foam structure (size and size distribution of the bubbles) [8,26]. For example, in the current study, the increase in the Young's modulus of the *F-C100* nanocomposite foams was as high as 82% compared to neat PMMA foams, whereas the increase in the Young's modulus of the corresponding unfoamed samples (*C100* vs. PMMA) was only 40%. The same comparison for the collapse strength yields values of 104% vs. 14%.

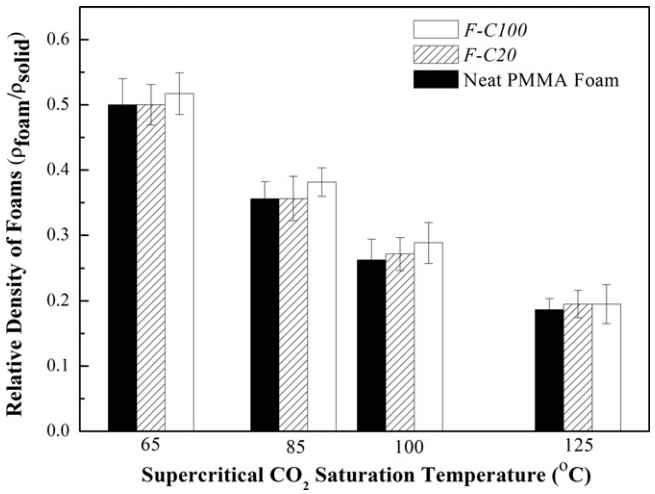

Fig. 5. The relative density ρ_r (ρ_{foam}/ρ_{solid}) of nanocomposites and neat PMMA foamed with supercritical CO_2 at 17.9 MPa and four different temperatures: (a) 65 °C, (b) 80 °C, (c) 100 °C and (d) 125 °C. The error bars represent the standard deviations of density of five specimens for each sample.

3.4.1. The influence of foam density on the mechanical properties of nanocomposite foams

In order to discuss the influence of foam density on the properties of nanocomposite foams, the influence of solid matrix properties is excluded by normalizing the Young's modulus (E_{foam}) and collapse strength (σ_{cl}) of the polymer foams by the Young's modulus (E_{solid}) and compressive strength (σ_{solid}) of the corresponding solid samples. The normalized values are termed the relative modulus ($E_r = E_{foam}/E_{solid}$) and the relative strength ($\sigma_r = \sigma_{cl}/\sigma_{solid}$).

The Gibson–Ashby model [26] is commonly used to quantitatively predict the mechanical properties of polymeric foams. In this model, the polymer foams are assumed to be composed of unit cells with cell edges, cell walls and gas inside the cells. All three components contribute to the mechanical properties of the foam. Under compression, the cell edges are bent, the cell walls are stretched and

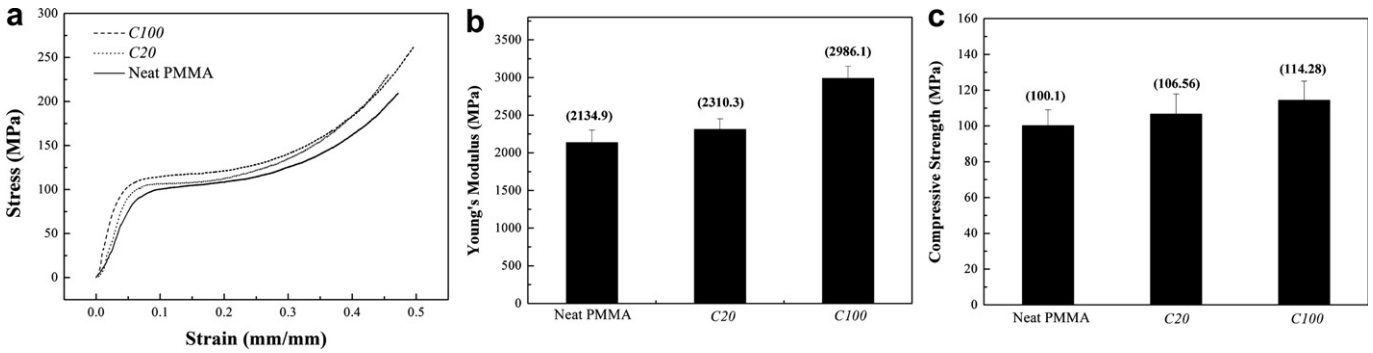

Fig. 4. (a) Typical compressive stress–strain curves for neat PMMA control sample and nanocomposites *C100* and *C20*. (b) A plot showing the Young's modulus of solid nanocomposites and neat PMMA. (c) A plot showing the compressive strength of solid nanocomposites and neat PMMA. The error bars represent the standard deviations of Young's modulus or collapse strength value of five specimens for each sample.

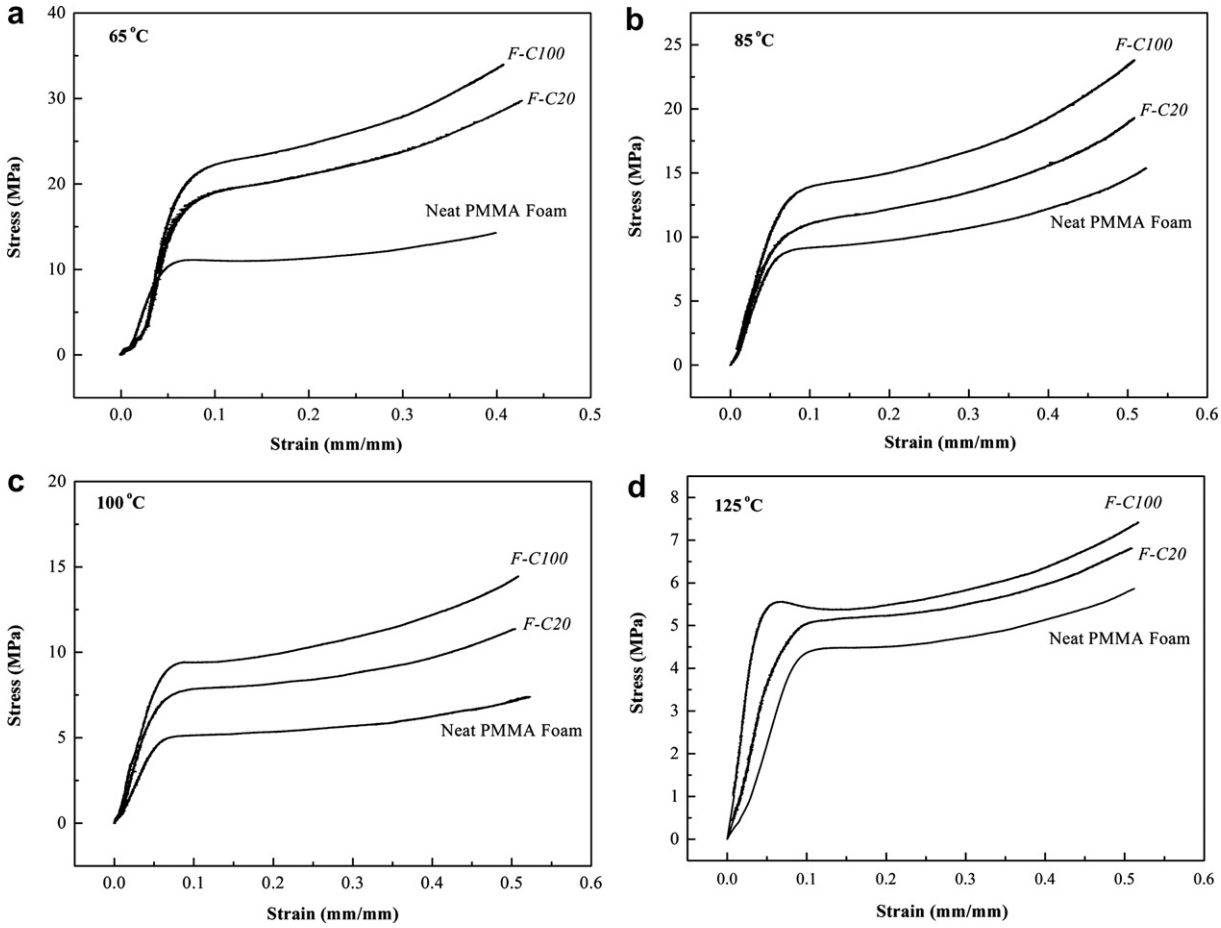

Fig. 6. Typical compressive stress–strain curves of nanocomposites *C100*, *C20* and neat PMMA foamed with supercritical CO_2 at 17.9 MPa and four different temperatures: (a) 65 °C, (b) 80 °C, (c) 100 °C and (d) 125 °C.

the gas inside the foams is compressed. The contribution from the gas compression is usually negligible when the gas pressure is atmospheric pressure. The Gibson–Ashby model describes the relationship between the relative properties of the polymer foams and the relative density as follows:

$$E_r = \phi^2 \cdot \rho_r^2 + (1-\phi)\cdot\rho_r \tag{2}$$

$$\sigma_r = \phi^{\frac{3}{2}} \cdot \rho_r^{\frac{3}{2}} + (1-\phi)\cdot\rho_r \tag{3}$$

where ϕ is the volume fraction of polymer used for constructing cell edges, and is used as a fitting constant. ρ_r is the relative density of foams, which is defined as the density of a foam divided by the density of its solid counterpart ($\rho_r = \rho_{foam}/\rho_{solid}$).

The predicted relative modulus by Eq. (2) is compared with the current experimental results of neat PMMA foams as well as nanocomposite foams in Fig. 8. By fitting Eq. (2) with the relative modulus of neat PMMA foam, which has a relative density of 0.186, the value of ϕ was calculated to be 0.9. Dashed line in Fig. 8 presents the fit of Eq. (2) with this value of $\phi = 0.9$. To demonstrate the change of the curve with the change of ϕ value, curves with

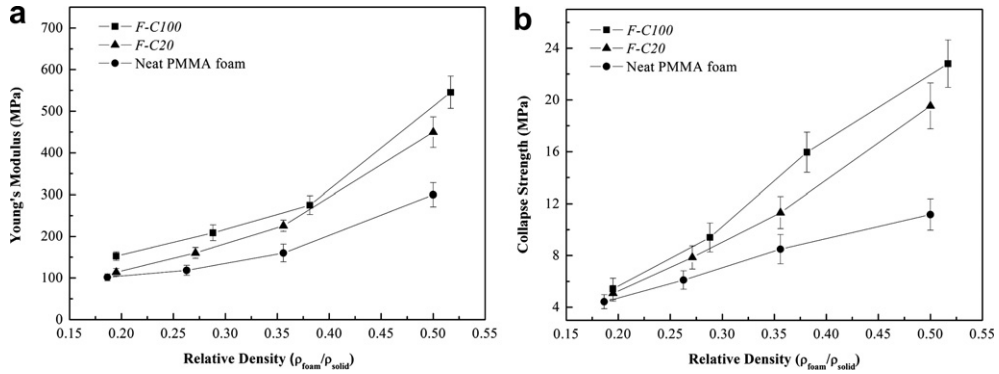

Fig. 7. Plots showing the change of (a) Young's modulus and (b) collapse strength of nanocomposites foams and neat PMMA foams with relative density. The error bars represent the standard deviations of Young's modulus/collapse strength of five specimens for each sample.

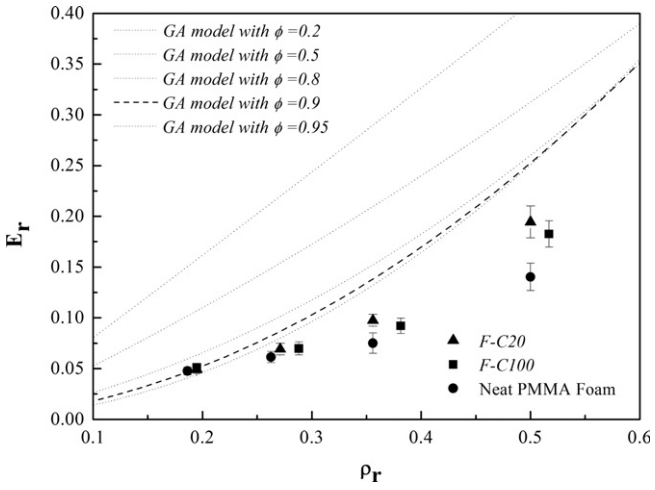

Fig. 8. A plot the change of relative modulus E_r with the change of relative density for *F-C100*, *F-C20* and neat PMMA foams. The broken line is the predicted curve by Gibson–Ashby model with $\phi = 0.9$. The dotted line is the Gibson–Ashby model with various ϕ value.

different ϕ values were also shown as dotted lines. It can be seen that the Gibson–Ashby model over-predicted the relative modulus of the polymer foams when the relative density was over 0.2. Such discrepancy is due to the simplified assumptions used in the Gibson–Ashby model. In this model, the foam was assumed to be composed of lattice or rod like structures in which cellular walls and struts were modeled as structural shell and beam elements, respectively. The aspect ratio of the walls and struts (strut length/cross section area, or wall area/wall thickness) was assumed to be large. However, when the relative density of the foam is high, such an assumption is no longer valid [9]. In addition, the ϕ value is a constant that does not depend on foam density. This may not be true for real samples. At high densities, it is very hard to determine the ϕ value by this model.

Naguib et al. [27] developed a constitutive model for characterizing the compressive behavior of PMMA open-cell foams. They assumed that the foam is comprised of cubic cages with equal dimensions, as shown in Fig. 9. They first calculated the relative density (ρ_r) of the foam based on the cubic unit, which is a function of the geometry (l and t) of the unit cell:

$$\rho_r = -2\left(\frac{t}{l}\right)^3 + 3\left(\frac{t}{l}\right)^2 \tag{4}$$

When compression loading was applied to the unit cell, the relative modulus of the foam (E_r) was obtained by using the same beam theory that was used in the Gibson–Ashby model [26]:

$$E_r = C_0\left(\frac{t}{l}\right)^4 \tag{5}$$

By combining Eqs. (4) and (5), and approximating the relationship of t/l with ρ_r in the range of $(0.2 \le \rho_r \le 0.8)$ by:

$$\frac{t}{l} = 0.1459 + 0.7082\rho_r$$

Naguib et al. obtained the following relationship:

$$E_r = C_0(0.14159 + 0.7082\rho_r)^4$$

where C_0 is a constant to be determined by fitting with experimental data. This model represented their experimental results very well. However, this model was based on an open-cell unit, in which only cell edges contribute to the mechanical reinforcement of foams. It is not applicable to predict the elastic modulus of closed-cell foams in which both cell walls and cell edges contribute to the mechanical reinforcement. As a result, a modified constitutive model based on closed-cell foams will be developed in the next section.

3.4.2. A modified constitutive model for predicting the mechanical properties of closed-cell polymer foams

Similar to the Naguib's model, the closed-cell foams are considered to be comprised of cubic unit cells as shown in Fig. 9(b). However, the unit cell for closed-cell foams is a cube with cell faces, as shown in Fig. 9(c) instead of cubic cages. To simplify the calculation, the face thickness (t_e) is assumed to be equal to the edge thickness (t_f) and $t_e = t_f = t/2$. The edge length is l. Then the volume of solid inside the edges (V_e) is:

$$V_e = 12\left(\frac{t}{2}\right)^2(l-t) + 8\left(\frac{t}{2}\right)^3 = 3t^2l - 2t^3 \tag{6}$$

The volume of solid inside the cell face is:

$$V_f = 6(l-t)^2\frac{t}{2} \tag{7}$$

The gas volume inside the cell is:

$$V_g = (l-t)^3 \tag{8}$$

The total volume of the unit cell is:

$$V_t = l^3$$

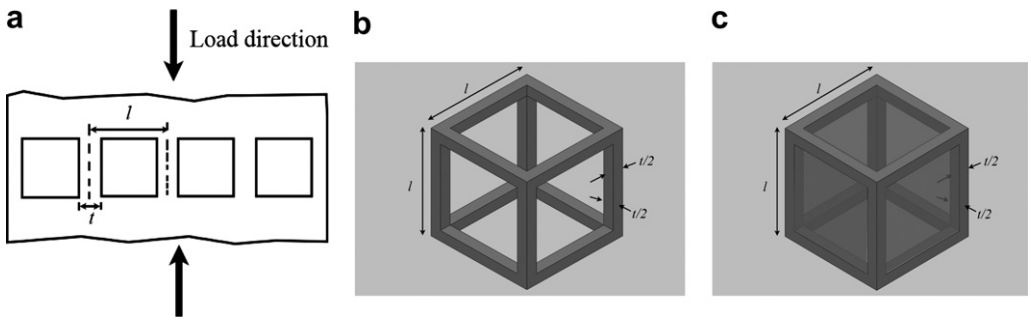

Fig. 9. Constitutive modeling of polymer foam: (a) macroscopic arrangement of unit cells inside the foam (b) the unit cell [27]. (c) A cubic unit cell for the constitutive model of closed-cell foams.

The density of the gas is very low compared to the density of the solid polymer that and is neglected in this model. The relative density ρ_r of the unit cell is:

$$\rho_r = \frac{V_{solid}}{V_{total}} = \frac{V_t - V_g}{V_t} = 1 - \frac{(l-t)^3}{l^3} = 1 - \left(1 - \frac{t}{l}\right)^3 \quad (9)$$

The volume fraction of polymer inside cell edges ϕ is:

$$\phi = \frac{V_e}{V_{solid}} = \frac{V_e}{1 - V_g} = \frac{3t^2 l - 2t^3}{l^3 - (l-t)^3} = \frac{3\left(\frac{t}{l}\right)^2 - 2\left(\frac{t}{l}\right)^3}{1 - \left(1 - \frac{t}{l}\right)^3} \quad (10)$$

According to beam theory, as detailed in the Gibson–Ashby model [26], the modulus contribution from the cell edges to the relative modulus of closed-cell foams is given by:

$$\frac{E'_e}{E_b} = \alpha\left(\frac{t_e}{l}\right)^4 \quad (11)$$

The modulus contribution from the cell face is given by:

$$\frac{E'_f}{E_b} = \beta\frac{t_f}{l} \quad (12)$$

So the relative modulus of the closed-cell foam is given by:

$$E_r = \alpha\phi\left(\frac{t_e}{l}\right)^4 + \beta(1-\phi)\frac{t_f}{l} \quad (13)$$

where α and β are constants of proportionality. Because it is assumed in this model that $t_e = t_f = t/2$, then:

$$E_r = \alpha\phi\left(\frac{t}{2l}\right)^4 + \beta(1-\phi)\frac{t}{2l} \quad (14)$$

By substituting ϕ with Eq. (10) into Eq. (14), the relative modulus is related to t/l by:

$$E_r = \alpha\left(\frac{3\left(\frac{t}{l}\right)^2 - 2\left(\frac{t}{l}\right)^3}{1\left(1 - \frac{t}{l}\right)^3}\right)\left(\frac{t}{2l}\right)^4 + \beta\left(1 - \frac{3\left(\frac{t}{l}\right)^2 - 2\left(\frac{t}{l}\right)^3}{1 - \left(1 - \frac{t}{l}\right)^3}\right)\frac{t}{2l}$$

If we define the inverse aspect ratio of cell edges, i.e. the ratio of the edge thickness (t) over edge length (l), as A_r, where $A_r = t/l$, then:

$$E_r = \alpha\left(\frac{3A_r^2 - 2A_r^3}{1 - (1 - A_r)^3}\right)\left(\frac{A_r}{2}\right)^4 + \beta\left(1 - \frac{3A_r^2 - 2A_r^3}{1 - (1 - A_r)^3}\right)\frac{A_r}{2} \quad (15)$$

It should be noted that $A_r \leq 1$. If $A_r = 1$, then the sample becomes a solid and $E_r = 1$. Applying this boundary condition to Eq. (15), yields $\alpha = 16$. Thus:

$$E_r = \left(\frac{3A_r^2 - 2A_r^3}{1 - (1 - A_r)^3}\right)A_r^4 + \beta\left(1 - \frac{3A_r^2 - 2A_r^3}{1 - (1 - A_r)^3}\right)\frac{A_r}{2} \quad (16)$$

According to Eq. (9), A_r can be calculated from ρ_r by:

$$A_r = 1 - (1 - \rho_r)^{\frac{1}{3}} \quad (17)$$

By combining Eqs. (16) and (17), the relative modulus of the closed-cell foams can be calculated from the relative density.

By substituting the experimental results of neat PMMA foam at $\rho_r = 0.186$ and $E_r = 0.0476$ into Eqs. (16) and (17), β is calculated to be 1.5. The relative modulus of various samples as a function of relative density is presented in Fig. 10 with the Gibson–Ashby fit ($\phi = 0.9$) and the model proposed in the current work (with $\beta = 1.5$). It can be seen from that the constitutive model proposed in the current work represents the experimental data quite well when the relative density is below 0.5. When the relative density is higher than 0.5, the model tends to underestimate the relative modulus. There are many possible reasons that can lead to this discrepancy. First, the assumption that the face thickness is equal to edge thickness is not true for real composites, and there is always a distribution of edge and face sizes in a foam. Second, at high density, when the inter cell distance is on the same order as the cell size, then the edge thickness is on the same order as the edge length, and beam theory is no longer applicable for calculating the elastic modulus. Third, the shape of the unit cell in real foams is never cubic. At high density (low bubble density), the cells tend to be spherical because they are separated instead of coalesced. And last, the relative modulus is calculated based upon the elastic modulus of bulk solid polymer and nanocomposites. The true value of E_{solid} is hard to get for polymer foams because the foaming process may also influence the properties of the polymer due to, for example, polymer-chain alignment [26]. However, the proposed constitutive model performs better than the Gibson–Ashby model in predicting the elastic modulus of closed-cell polymer foams in the medium density range ($0.2 \leq \rho_r \leq 0.5$).

The relative strength of closed-cell polymer foams can also be predicted by the proposed constitutive model. According to the beam theory, the contribution of the cell edge to the collapse strength can be described by:

$$\frac{\sigma_e}{\sigma_y} = \alpha'\left(\frac{t_e}{l}\right)^3$$

where α' is a constant of proportionality, and σ_y is the yield stress of the solid material. The contribution of the cell face to the collapse strength can be described by:

$$\frac{\sigma_e}{\sigma_y} = \beta'\frac{t_f}{l}$$

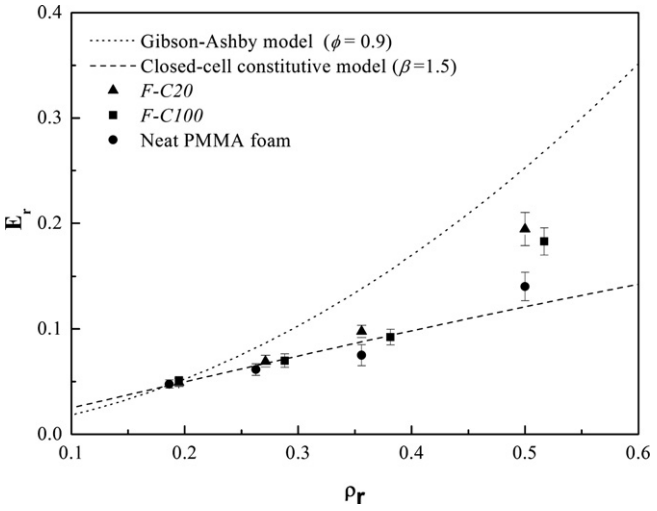

Fig. 10. A comparison of Gibson–Ashby model and closed-cell constitutive model predicted relative modulus with the experimental results of *F-C100*, *F-C20* and neat PMMA foams.

Therefore, the relative strength (σ_r) of the polymer foam is given by:

$$\sigma_r = \alpha'\phi\left(\frac{t_e}{l}\right)^3 + (1-\phi)\beta'\frac{t_f}{l}$$

In the proposed model, $t_e = t_f = t/2$, and ϕ is given by Eq. (9), therefore, the relative strength is given by:

$$\sigma_r = \alpha'\left(\frac{3\left(\frac{t}{l}\right)^2 - 2\left(\frac{t}{l}\right)^3}{1-\left(1-\frac{t}{l}\right)^3}\right)\left(\frac{t}{2l}\right)^3 + \beta'\left(1 - \frac{3\left(\frac{t}{l}\right)^2 - 2\left(\frac{t}{l}\right)^3}{1-\left(1-\frac{t}{l}\right)^3}\right)\frac{t}{2l}$$
$$= \frac{\alpha'}{8}\left(\frac{3A_r^2 - 2A_r^3}{1-(1-A_r)^3}\right)A_r^3 + \frac{\beta'}{2}\left(1 - \frac{3A_r^2 - 2A_r^3}{1-(1-A_r)^3}\right)A_r \quad (18)$$

When $A_r = 1$, the foam becomes a solid, and $\sigma_r = 1$. Thus α' is calculated to be 8. The value of β' is calculated to be 1.3 by fitting Eqs. (17) and (18) to the relative density and relative strength of neat PMMA foamed at 125 °C. Using these α' and β' values, the change of foam relative strength with relative density can be predicted by the combination of Eqs. (17) and (18). The predicted relative strength is presented in Fig. 11 along with the Gibson–Ashby model ($\phi = 0.9$). Both the Gibson–Ashby model and the proposed model fit the experimental results of neat PMMA foams well when the relative density is lower than 0.3, but at higher densities, the proposed constitutive model represents the experimental data better than the Gibson–Ashby model.

The experimental results of the relative strength of nanocomposite foams (*F-C20* and *F-C100*) are greater than both the Gibson–Ashby and the proposed model predictions. This is possibly due to the small cell size of the nanocomposite foam due to the presence of nanofillers as nucleating agents. As the cell size gets smaller, the beam-bending concept breaks down because the cell walls become short and squat and they yield axially before they bend.

3.4.3. The influence of cell size on the compressive properties of polymer foams

It was found that the relative modulus of the nanocomposite foams is higher than that of neat PMMA foam particularly at high relative densities (Fig. 10). In addition, the relative modulus of *F-C20* foams is higher than that of *F-C100* foams. Since the relative modulus is normalized by the elastic modulus of the solid material (neat PMMA), the observed deviation in the relative modulus should not have been caused by differences in elastic modulus of the solid material but rather should be due to differences in the foam morphology of the foams.

Table 2
Average cell face thickness, A_r, value and relative density for neat PMMA foams, *C100* foams and *C20* foams foamed with supercritical CO_2 saturation temperature at 65 °C.

	Neat PMMA	*C100*	*C20*
Bubble wall thickness (t) (μm)	0.73	0.482	0.475
Average bubble size (l') (μm)	4.94	2.42	1.34
A_r (t/l')	0.148	0.195	0.355
Relative density (ρ_r)	0.50	0.52	0.50

In Table 1, the average bubble radii of *F-C100*, *F-C20* and neat PMMA foamed at various temperatures are summarized. According to Figs. 2 and 8, the relative density of the nanocomposites and neat PMMA foamed under the same conditions is similar, but the bubble size differs. *F-C20* foams always have the smallest bubble size and neat PMMA foams always have the largest bubble size at the same relative density. When the relative density is low, the relative modulus of both nanocomposite foams and neat PMMA foams are the same suggesting that the influence of bubble size on the relative modulus is negligible at low relative densities. However, when the relative density is high, the influence of bubble size on the relative modulus becomes significant.

In the proposed constitutive model, the relative density (ρ_r) is a function of cell edge inverse aspect ratio, A_r (t/l). And Eq. (17) suggests a one-to-one relationship between A_r and ρ_r, which means that, at the same density, the ratio of cell edge length and edge thickness is constant. Thus, one relative density can only lead to one predicted relative modulus, without the influence of unit cell size (l).

However, the experimental results show that at the same relative density, there can be more than one value of relative modulus. This discrepancy is possibly due to the simple cubic unit that was used in the derivation of the constitutive model. In real foams, the cells are formed with various kinds of three dimensional shapes,

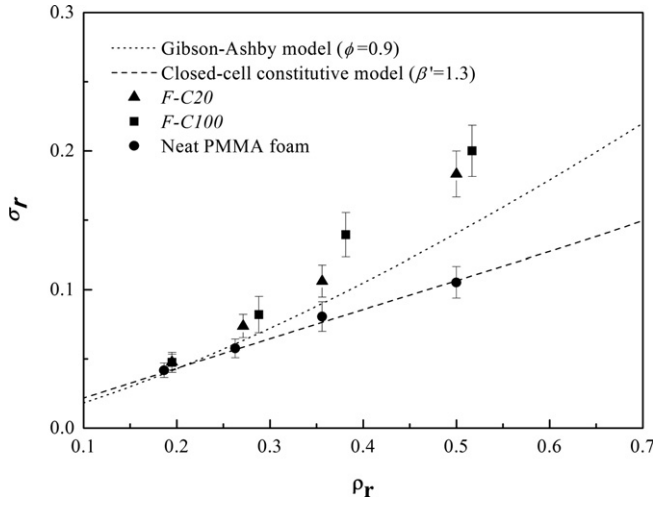

Fig. 11. A comparison of Gibson–Ashby model and closed-cell constitutive model predicted relative strength with the experimental results of *F-C100*, *F-C20* and neat PMMA foams.

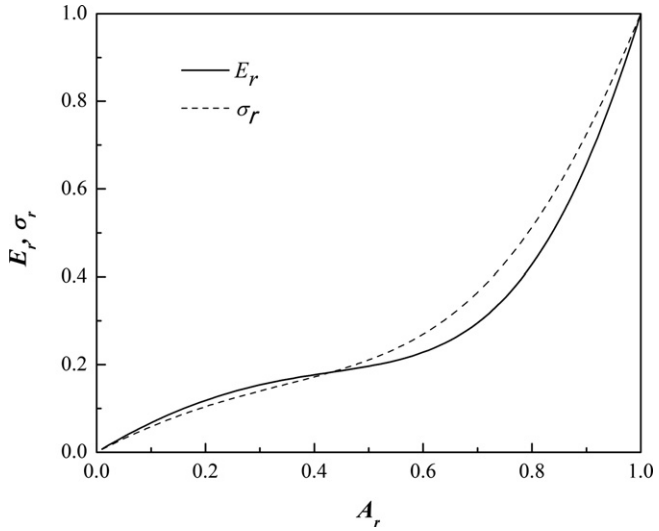

Fig. 12. A plot showing the change of relative modulus and relative strength with A_r predicted by closed-cell constitutive model for cubic cell shape.

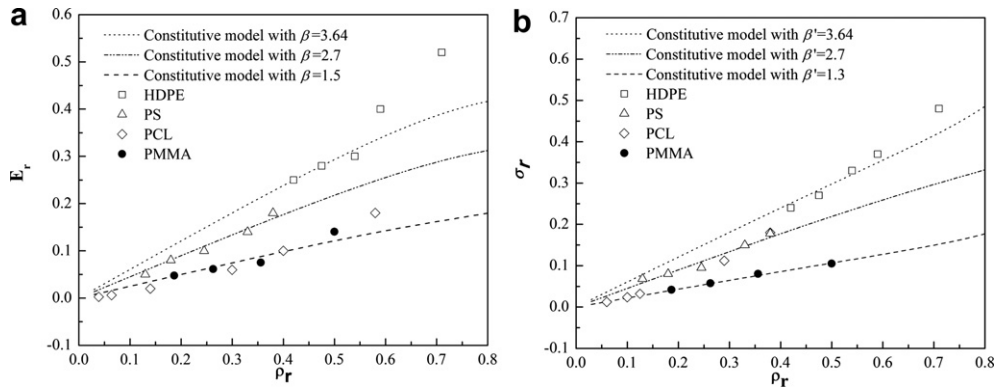

Fig. 13. A comparison between the relative modulus and relative strength from prior research results and the results predicted by the closed-cell constitutive model.

such as spheres, square prism, rhombic dodecahedra and tetrakaidecahedra. Each of these shapes has a different ρ_r vs. A_r relationship. For example, the relative density of rhombic dodecahedra is given by Ref. [26]:

$$\rho_r = 1.9\frac{t}{l} = 1.9A_r$$

And the relative density of tetrakaidecahedra is given by:

$$\rho_r = 1.18\frac{t}{l} = 1.18A_r$$

Even if the relative density is the same, the difference in cell shapes will lead to differences in A_r values, thus leading to differences in the relative modulus.

The average bubble edge thickness was measured using the FESEM images of the fracture surfaces of neat PMMA foams, *F-C100* foams and *F-C20* foams at 65 °C. For each sample, the thickness of 100 bubble edges was measured and the average value is summarized in Table 2. The average bubble size (l') and relative mass density (ρ_r) are also listed. It should be noted that the bubble size was calculated from the cross sectional area of cells based on the assumption that the bubbles were spherical. So the bubble size listed in Table 2 is not equivalent to the cell edge length (l) in the closed-cell constitutive model. However, the value of A_r should still be proportional to the value of t/l'. It can be seen that both the neat PMMA foam and the *F-C20* foam have the same relative density (0.5), but the *F-C20* foam has a much higher A_r value than neat PMMA foam. Based on Eqs. (16) and (18), the change of relative modulus and relative strength with A_r is plotted in Fig. 12. It can be seen that the relative modulus and relative strength increase with increasing A_r. A thick and short strut with high A_r value is more difficult to bend than a thin and long strut with low A_r value. As a result, the *F-C20* foams have higher relative modulus and relative strength than both *F-C100* and neat PMMA foams.

3.4.4. Applicability of the proposed model to literature data

The proposed constitutive model was used to fit the prior mechanical testing results of other polymer foams such as polystyrene (PS) [28], high density polyethylene (HDPE) [29] and poly(ϵ-caprolactone) [30]. The results are shown in Fig. 13. The current research results of neat PMMA are also included for comparison. It can be seen that by fitting the new model with the experimental results, the values of β and β' for different materials can be determined. The curves predicted by the proposed closed-cell constitutive model fit very well with the relative modulus and relative collapse strength of different polymer foams when the relative density is lower than 0.5.

4. Conclusions

In the current research, the compressive properties of multi-walled carbon nanotube/poly(methyl methacrylate) (MWNT/PMMA) nanocomposite foams were studied. The Young's modulus and collapse strength of PMMA foams increased significantly with the addition of 1% MWNT by weight. The addition of MWNTs influenced the properties of nanocomposite foams not only by influencing the matrix properties, but also by influencing the foam morphology. Under the same foaming conditions, the PMMA foams filled with long MWNTs (*F-C100*) showed greater Young's modulus and collapse strength values than the PMMA foams filled with short MWNTs (*F-C20*). However, the relative modulus and relative strength (relative with respect to unfoamed nanocomposite) of the *F-C20* foam is greater than those of the *F-C100* foam. The bubble density of *F-C20* foams was found to be greater than that of *F-C100*, which led to smaller average bubble size in *F-C20*. Therefore, we conclude that the differences observed in the compressive properties were directly related to the foam morphology of the foamed nanocomposite.

A modified constitutive model for predicting the compressive mechanical properties of closed-cell polymer foams was developed. The Young's modulus and collapse strength predicted by the new model fit the experimental results better than the Gibson–Ashby model. The proposed constitutive model can be used to predict the compressive mechanical properties of polymer foams with relative densities lower than 0.5.

The influence of cell (bubble) size on the mechanical properties of polymer foams was discussed using the proposed constitutive model. It was found that at constant relative density, foams with smaller cell sizes have greater Young's modulus and collapse strength than those with larger cell sizes. It was also found that at constant relative density, the wall thickness to cell size ratio (A_r) increased when the cell size decreased, which led to greater relative modulus values.

Acknowledgments

Financial support from the Nanoscale Science and Engineering Initiative of the National Science Foundation under NSF Award Number DMR-0117792 and CMMI-0500324 is gratefully acknowledged.

References

[1] Lee LJ, Zeng C, Cao X, Han X, Shen J, Xu G. Polymer nanocomposite foams. Compos Sci Technol 2005;65(15–16):2344–63.
[2] Han X, Zeng C, Lee LJ, Koelling KW, Tomasko DL. Extrusion of polystyrene nanocomposite foams with supercritical CO_2. Polym Eng Sci 2003;43(6):1261–75.

[3] Siripurapu S, DeSimone JM, Khan SA, Spontak RJ. Controlled foaming of polymer films through restricted surface diffusion and the addition of nanosilica particles or CO_2-philic surfactants. Macromolecules 2005;38(6):2271–80.
[4] Zhai W, Yu J, Wu L, Ma W, He J. Heterogeneous nucleation uniformizing cell size distribution in microcellular nanocomposites foams. Polymer 2006; 47(21):7580–9.
[5] Goren BK, Chen L, Schadler L, Ozisik R. Influence of nanoparticle surface chemistry and size on supercritical carbon dioxide processed nanocomposite foam morphology. J Supercritical Fluids 2010;51(3):420–7.
[6] Thomassin JM, Pagnoulle C, Bednarz L, Huynen I, Jerome R, Detrembleur C. Foams of polycaprolactone/MWNT nanocomposites for efficient EMI reduction. J Mater Chem 2008;18(7):792–6.
[7] Dai X, Liu Z, Wang Y, Yang G, Xu J, Han B. High damping property of microcellular polymer prepared by friendly environmental approach. J Supercritical Fluids 2005;33(3):259–67.
[8] Saha MC, Mahufz H, Chakravarty UK, Udin M, Kabir MdE, Jeelani S. Effect of density, microstructure, and strain rate on compression behavior of polymeric foams. Mater Sci Eng A 2005;406(1–2):328–36.
[9] Alveraz P, Mendizabal A, Petite M, Rodriguez-Perez MA, Echeverria A. Finite element modelling of compressive mechanical behaviour of high and low density polymeric foams. Mat-wiss u Werkstofftech 2009;40(3):126–32.
[10] Saint-Michel F, Chazeau L, Cavaillé J, Chabert E. Mechanical properties of high density polyurethane foams: I. Effect of the density. Compos Sci Technol 2006; 66(15):2700–8.
[11] Kabir MdE, Saha MC, Jeelani S. Tensile and fracture behavior of polymer foams. Mater Sci Eng A 2006;429(1–2):225–35.
[12] Saha MC, Kabir MdE, Jeelani S. Effect of nanoparticles on mode-I fracture toughness of polyurethane foams. Polym Compos 2009;30(8):1058–64.
[13] Mahfuz H, Rangari VK, Islam MS, Jeelani J. Fabrication, synthesis and mechanical characterization of nanoparticles infused polyurethane foams. Composites Part A 2004;35(4):453–60.
[14] Shen J, Zeng C, Lee LJ. Synthesis of polystyrene–carbon nanofibers nanocomposite foams. Polymer 2005;46(14):5218–24.
[15] Moniruzzaman M, Winey KI. Polymer nanocomposites containing carbon nanotubes. Macromolecules 2006;39(16):5194–205.
[16] Yang Y, Gupta MC, Dudley KL, Lawrence RW. Conductive carbon fiberpolymer foam structures. Adv Mater 2005;17(16):1999–2003.
[17] Yang YL, Gupta MC. Novel carbon nanotube-polysterene foam composites for electromagnetic interference shielding. Nano Lett 2005;5(11):2131–4.
[18] Bauhofer W, Kovacs JZ. A review and analysis of electrical percolation in carbon nanotube polymer composites. Compos Sci Technol 2009;69(10): 1486–98.
[19] Chen L, Ozisik R, Schadler LS. The influence of carbon nanotube aspect ratio on the foam morphology of MWNT/PMMA nanocomposite foams. Polymer 2010; 51(11):2368–75.
[20] Wong KKH, Zinke-Allmang M, Hutter JL, Hrapovic S, Luong JHT, Wan W. The effect of carbon nanotube aspect ratio and loading on the elastic modulus of electrospun poly(vinyl alcohol)-carbon nanotube hybrid fibers. Carbon 2009; 47(11):2571–8.
[21] Bult J. Controlled carbon nanotube synthesis for quantification of polymer-nanotube composite Micromechanics. PhD Thesis: Rensselaer Polytechnic Institute; 2007, p. 19.
[22] Gross S, Camozzo D, Noto VD, Armelao L, Tondello E. PMMA: a key macromolecular component for dielectric low-κ hybrid inorganic-organic polymer films. Eur Polym J 2007;43(4):673–96.
[23] Bahr JL, Tour JM. Covalent chemistry of single-wall carbon nanotubes. J Mater Chem 2002;12(7):1952–8.
[24] Eitan A, Fisher FT, Andrews R, Brinson LC, Schadler LS. Reinforcement mechanisms in MWCNT-filled polycarbonate. Compos Sci Technol 2006;66: 1162.
[25] Duncan R. Characterizing the reinforcement mechanisms in multiwall nanotube/polycarbonate composites across different length and time scales. PhD Thesis: Rensselaer Polytechnic Institute; 2008.
[26] Gibson LJ, Ashby MF. Cellular solids: structure and properties. 2nd ed. New York: Cambridge University Press; 1997. p. 195–207.
[27] Jo C, Fu J, Naguib HE. Constitutive modeling for characterizing the compressive behavior of PMMA open-cell foams. J Polym Science Part B Polym Phys 2007;45:436.
[28] Doroudiani S, Kortschot MT. Polystyrene foams. III: structure–tensile properties relationships. J Appl Polym Sci 2003;90:1427.
[29] Zhang Y, Rodrigue D, Ait-Kadi A. High density polyethylene foams. III. Tensile properties. J Appl Polym Sci 2003;90:2130.
[30] Liu H, Han C, Dong L. Study on the cell structure and compressive behavior of biodegradable poly(ϵ-caprolactone) foam. Polym Eng Sci 2008;12:2432.